Measurements and ALE3D Simulations for Violence in a Scaled Thermal Explosion Experiment with LX-10 and AerMet 100 Steel

M. A. McClelland, J. L. Maienschein, J. J. Yoh, M. R. deHaven, O. T. Strand

June 10, 2005

Disclaimer

Measurements and ALE3D Simulations for Violence in a Scaled Thermal Explosion Experiment with LX-10 and AerMet 100 Steel*

M. A. McClelland, J. L. Maienschein, J. J. Yoh,
M. R. deHaven, and O. T. Strand
Lawrence Livermore National Laboratory

ABSTRACT

We completed a Scaled Thermal Explosion Experiment (STEX) and performed ALE3D simulations for the HMX-based explosive, LX-10, confined in an AerMet 100 (iron-cobalt-nickel alloy) vessel. The explosive was heated at 1 °C/h until cookoff at 182 °C using a controlled temperature profile. During the explosion, the expansion of the tube and fragment velocities were measured with strain gauges, Photonic-Doppler-Velocimeters (PDVs), and micropower radar units. These results were combined to produce a single curve describing 15 cm of tube wall motion. A majority of the metal fragments were captured and cataloged. A fragment size distribution was constructed, and a typical fragment had a length scale of 2 cm. Based on these results, the explosion was considered to be a violent deflagration.

ALE3D models for chemical, thermal, and mechanical behavior were developed for the heating and explosive processes. A four-step chemical kinetics model is employed for the HMX while a one-step model is used for the Viton. A pressure-dependent deflagration model is employed during the expansion. The mechanical behavior of the solid constituents is represented by a Steinberg-Guinan model while polynomial and gamma-law expressions are used for the equation of state of the solid and gas species, respectively. A gamma-law model is employed for the air in gaps, and a mixed material model is used for the interface between air and explosive. A Johnson-Cook model with an empirical rule for failure strain is used to describe fracture behavior. Parameters for the kinetics model were specified using measurements of the One-Dimensional-Time-to-Explosion (ODTX), while measurements for burn rate were employed to determine parameters in the burn front model. The ALE3D models provide good predictions for the thermal behavior and time to explosion, but the predicted wall expansion curve is higher than the measured curve. Possible contributions to this discrepancy include inaccuracies in the chemical models, integration of the momentum equation, and representation of the interfaces in the gaps. Two model problems were used to explore the effects of parameter variations on the fracture and fragmentation of AerMet 100 tube sections driven by the deflagration of LX-10. For the range of parameters considered, the model fragment sizes are of the same scale as the measured sizes.

INTRODUCTION

Computational tools are being developed to predict the response of munitions and propellant systems to thermal (cookoff) events. These simulation tools are needed to help answer questions related to fire hazards in a climate of tighter restrictions concerning safety and protection of the environment. Applications include systems with insensitive munitions, the development of sub-scale fire tests for rocket motors, the shipboard storage of munitions, fire-fighting strategies, and the development of laser weapons systems.

Lawrence Livermore National Laboratory[1-3] (LLNL), Sandia National Laboratory[4] (SNL), the Naval Air Warfare Center[5, 6] (NAWC), and the Naval Surface Warfare Center[7] (NSWC) have been performing benchmark cookoff experiments and developing simulation models and tools. Recently, these laboratories completed a joint effort to validate cookoff models. Materials were characterized[8], small[5]-

and large-scale[6] cookoff experiments were performed, and models results were compared with measurements[3, 4]. The models provided good representations of measurements for thermal fields and time to explosion. Although the modeling work did not yield satisfactory predictions for violence, they did help to guide follow-on efforts.

We have been investigating cookoff behavior for a number of explosives in the STEX system[2] shown in Figure 1. A sealed tube with heavily-reinforced ends is heated slowly until ignition occurs. The response is characterized using thermocouples, strain gauges, PDV probes, and radar units to measure fragment velocities. The geometry of this cookoff system is relatively simple to facilitate model and code development. An effort is being made to characterize a wide range of physical processes and achieve a range of results for reaction violence.
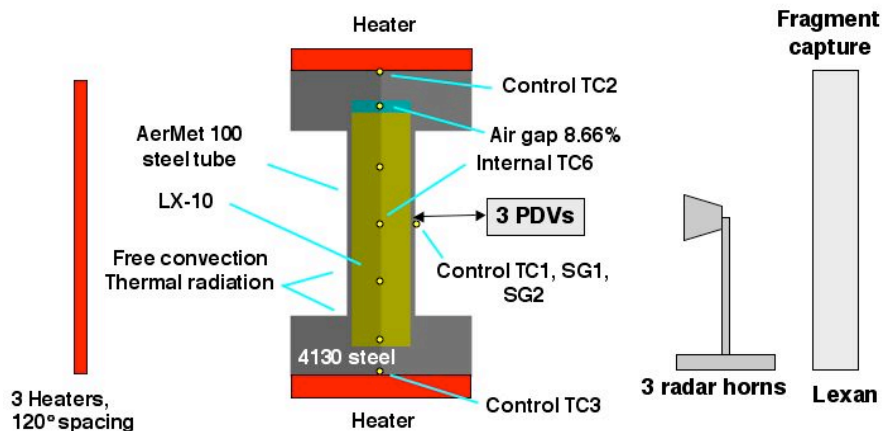

Figure 1 Schematic of geometry and instrumentation for STEX cookoff test TE-047 for LX-10 in an AerMet 100 vessel.

We have developed ALE3D chemical, mechanical, and thermal models to predict the thermal behavior, time to explosion, and violence for PBXN-109[3] (64% RDX, 20% Al, 16% DOA/HTPB), C4[3] (91% RDX, 7% fuel oil 2% PIB), and Comp B[9] (64% RDX, 36% TNT) in STEX experiments. Good predictions for the time to explosion were obtained in all cases. The measured temperature fields were well modeled for PBXN-109 and C4, but not for Comp B. For Comp B, the buoyant liquid TNT is believed to have altered the temperature fields, and will need to be included in future models. In order to assess predictive capabilities for violence, measured and predicted wall strains were compared during the slow heating and explosive phases. For PBXN-109, the measured strains were well described by the models during both the heating and explosive phases. For C-4, the predicted strains were higher than the measurements. This discrepancy was most likely the result of numerical errors from the mass scaling method used to integrate the momentum equation combined with relatively light confinement, which magnifies the errors. For Comp B, model predictions for the expansion were satisfactory during the slow heating phase, but increased much faster than the measured expansion during the explosive phase. In this paper, we turn our attention to an HMX-based explosive and present STEX measurements of time to explosion, thermal behavior, and violence for LX-10 confined in an AerMet 100 vessel. These measurements are compared with initial predictions from an ALE3D model. In addition, we give parametric results for two model problems involving the fracture of AerMet 100 driven by the deflagration of LX-10.

SCALED THERMAL EXPLOSION EXPERIMENTS FOR LX-10/AERMET 100

In order to provide extensive violence measurements for benchmarking our ALE3D models for slow cookoff, we completed a STEX test (TE-047) for LX-10-2 confined in an AerMet 100 vessel. LX-10-2 (94.7% HMX, 5.3% Viton A) is similar to the Navy's PBXN-5 which has nearly the same composition, but wider tolerances on the particle size distribution. This HE has a single energetic constituent, HMX, and has a small amount of an unreactive binder, Viton A. Detailed chemical, thermal, and mechanical models are available for HMX and mixtures of HMX and Viton A[10]. Also, this material can provide a range of violence results which is needed for thorough testing of the ALE3D models. The AerMet 100 steel (71% Fe, 13.4% Co, 11.1% Ni, 3% Cr, other) is

being studied as part of an MOU project on dynamic fracture and fragmentation[11]. Detailed ALE3D models have been developed for the fragmentation of this steel and are incorporated into our models as described below.

Experimental configuration

The vessel for this STEX test (TE-047) consists of the AerMet 100 tube with heavily reinforced end flanges made of 4130 steel (see Figure 1). The end seals are achieved with O-rings bolted between flanges. The AerMet 100 tube (4.493 cm ID X 20.32 cm L) was provided to us by the MOU project on fracture and fragmentation[11]. They heat-treated the tube to give a Rockwell C hardness of 55. The wall thickness was 0.293 cm giving a confinement pressure of 255 MPa. It was joined by friction welding to the standard STEX flanges made of 4130 steel [2].   This method of joining was utilized to avoid heating the entire tube and altering the heat treatment and the confinement characteristics

The LX-10 was pressed into five cylinders with a diameter of 4.36 cm, a combined length of 19.74 cm, and a density of 1.86 g/cm^3. The ullage of 8.66% was provided to allow the LX-10 to expand and change from the β to δ phase without the solid alone pressurizing the vessel cavity.

The temperature was measured at five internal locations using a probe and a number of external locations on the outer tube surface using Resistance Temperature Detectors (RTDs) (see Figure 1). Three Proportional-Integral-Derivative (PID) controllers were used to adjust the heater powers in the top, bottom, and set of three side heaters to keep respective thermocouples at top (TC2), bottom (TC3), and side (TC1) locations near their set-point values. In this experiment, the final ramp rate for the set-point temperature was 1 ^{o}C/h after the temperature was held at 130 ^{o}C for 5 hours (see Figure 2).
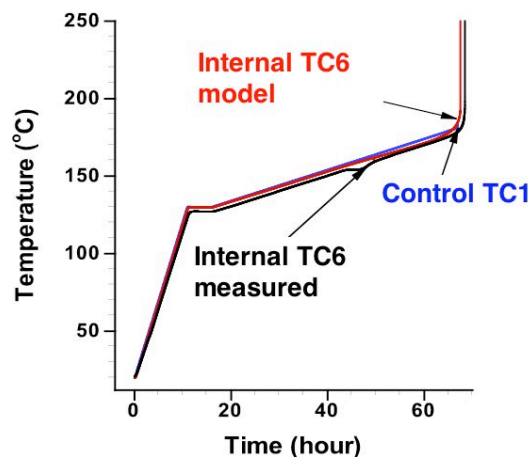

Figure 2 Measured and ALE3D model temperature results for STEX test TE-047 with LX-10 confined in an AerMet 100 vessel

Explosion violence was characterizing by capturing fragments and measuring the wall velocity at several stages of the explosion using strain gauges, PDV probes, and micropower radar systems. Two hoop (SG1, SG2) strain gauges with maximum ranges of 8 and 2%, respectively, were used to measure the deformation of the tube near the axial midplane during the entire thermal ramp and subsequent explosion. Three PDV probes, spaced at 120°, were used to measure the wall motion of the tube at the axial midplane over a 1.6 msec period during the explosion. Three radar systems with 120° spacing were used to measure the velocity of fragments at the axial midplane during the last stage of the measurement window. The rapid sampling of the strain gauges, PDV probes, and radar signals was triggered by break wires running the length of the vessel at the outside radius of the flanges. In order to capture data prior to the wire break, the data was looped through the oscilloscopes. Finally, fragments were captured in Lexan panels located on the four sides and ceiling of the shrapnel catcher.

Experimental results

The thermal explosion occurred at 182 °C as measured by the control thermocouple TC1 (see Figure 2). The center thermocouple TC 6 lagged TC1 by approximately 3 °C. The curve for TC 6 also shows a variation

from its linear increase at a temperature of approximately 155 °C which is the result of the endothermic β to δ phase transition. This temperature is somewhat lower than an expected value of 160 °C.

The violence observed in STEX TE-047 was consistent with a deflagration, but was still at the high end of the range of results for earlier experiments[12]. The explosion damaged structural components in the shrapnel catcher and displaced supports holding the top Lexan panel in place. The end flanges and bolts were distorted, but there was no flow of metal that would indicate a detonation (see Figure 3).

Figure 3 Loose fragments and end flanges for STEX test TE-047 with LX-10 confined in an AerMet 100 vessel

We recovered 106 AerMet 100 fragments with a total mass comprising 78% of the AerMet 100 tube mass between the flanges. There were 35 fragments imbedded in the Lexan panels, and the balance was collected as loose fragments. The fragment mass distribution is shown in the histogram of Figure 4. The median fragment mass was 2.2 g and a typical fragment had a dimension of 2 cm. Based on the average final thickness of the fragments, the real strain at fracture was approximately 15% (14% engineering strain).

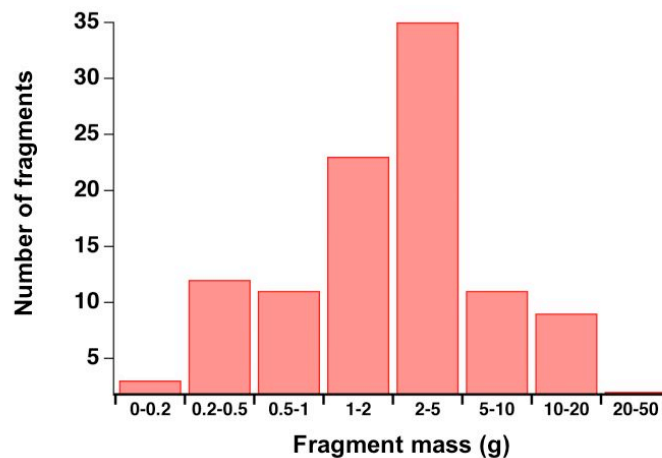Figure 4 Histogram of fragment masses for STEX test TE-047 with LX-10 confined in an AerMet 100 vessel

The tube wall velocity measurements from the three PDV probes and radar systems are plotted in Figure 5 versus time relative to the trigger point. The PDV measurements span nearly four orders of magnitude. For velocities less than 1 m/s, there are significant differences between the results for the three PDV probes,

suggesting some asymmetry in the early expansion. There is also more uncertainty in the measurements at these low velocities as evidenced by the increased measurement noise as the limits of the sensor are approached.   At the larger velocities, the three probes deliver very similar results, indicating remarkable symmetry in the expansion of the tube. The maximum measured PDV velocity is 770 m/s as given by probe no. 2. The three radar systems gave velocities of 1320, 1300, 940, and 1000 m/s with a mean of 1200 m/s. Note that the last two velocities are two measurements from horn no. 3, and are each given half weight in the calculation of the mean. The radar measurements continue the curve formed by the three PDV probes. The explosion occurs on the scale of 200 μs, indicating a deflagration. Also, an earlier defined average[12] $v_{avg}=v_{mean}/(1+\sigma_{vel}/v_{mean})$ has a value of 1030 m/s which is somewhat less than the values of 1200 and 1600 m/s for earlier two STEX tests[12] involving the detonation of β-phase PBX-9501. Here σ_{vel} is the standard deviation for the radar velocities.
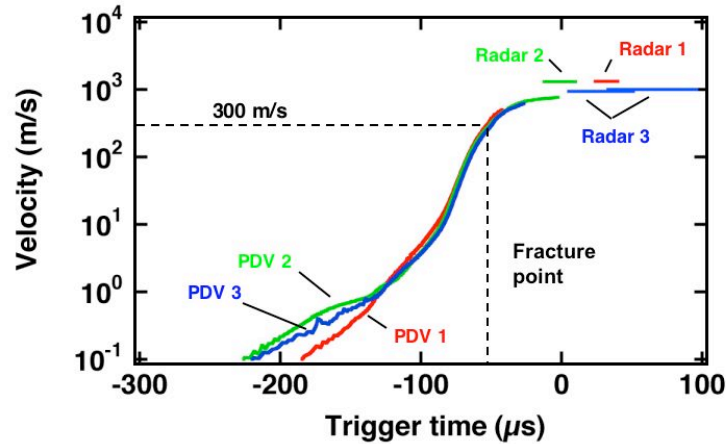

Figure 5 Tube wall velocity measurements from PDV and radar for STEX test TE-047 with LX-10 confined in an AerMet 100 vessel

Strain gauge, PDV, and radar results for the position of the tube wall and resulting fragments are plotted versus time in Figure 6. The initial position for SG2 and the three PDV probes is taken to be the measurement given by the strain gauge SG1. The gauge SG1 is believed to provide the best measurement during the rapid expansion.   This initial position has uncertainties of the scale ± 0.03 mm (± 0.1%). The measurements for gauges SG1 and SG2 were shifted forward in time by 3.6 and 77.9 ms to give the results of Figure 5. These very large time shifts raise question concerning the interpretation of the strain gauge measurements. At this time, it is believed that the measured times are incorrect and were the result of instrumentation errors. It is also possible that these expansions occurred earlier in time.   However, there is not yet a plausible physical scenario which would account for this behavior. With the time shifts performed, the SG1 and SG2 curves give very similar results and show smooth increases until their failure points at 3.4 and 1.8%, respectively.

The PDV curves were obtained by integrating the velocity curves of Figure 5 using the initial position from SG1. The PDV curves were extended using the average radar velocity and the final wall position calculated from PDV2. The linear expansion of the tube wall relative to the room temperature position is plotted on the right scale. The results from the two strain gauges, three PDV probes, and three radar systems provide a single curve for 15 cm of wall motion, corresponding to a 600% expansion. The outstanding question concerns the time shift of the strain gauge results discussed earlier. At the fracture limit of 14%, the PDV velocity is approximately 300 m/s (see Figure 5). Since velocities increase to 1200 m/s, there is considerable acceleration after fracture. These results suggest that both measurements and models need to include behavior after fragmentation to characterize violence.

ALE3D MODEL

AerMet 100 model

In the STEX test described above, the end caps were fabricated from 4130 steel and the tube section was made from AerMet 100. Steinberg-Guinan strength models were employed for both materials. A 7-term polynomial EOS was employed for the 4130 steel while a Gruniesen EOS was used

for the AerMet 100. The MOU Fracture and Fragmentation project group provided us with the AerMet 100 strength, EOS, and a detailed metal fracture model for use with ALE3D[13]. The metal fracture model is not included in the STEX simulations given below, but is employed in two test problems described at the end of this section. The metal fracture model is based on the Johnson and Cook[14] computational failure model. An empirical rule for failure strains was proposed by Hancock and McKenzie[15]:

$$\varepsilon_f = D_1 + D_2 \exp[D_3(-p/\sigma_v)] \tag{1}$$

Here D_1, D_2, and D_3 are material parameters, σ_v is the effective stress, and p is the pressure. An initial set of parameters were specified for AerMet 100[13]. These failure strains represent defects in the form of voids resulting from inclusions, defects, and impurities. In the physical system, these voids increase in size with tensile stress and plastic strain, and eventually link and form cracks. In the ALE3D model, a Gaussian distribution of failure strains is randomly spread over the AerMet 100 computational domain. There is a failure strain assigned to each computational element. When the failure strain is reached, the element "fails" and no longer supports a load. The failed zones merge to form cracks and finally fragments. At present, simulations can proceed until HE product gas begins to flow between the fragments and computational zones become excessively deformed as discussed below.
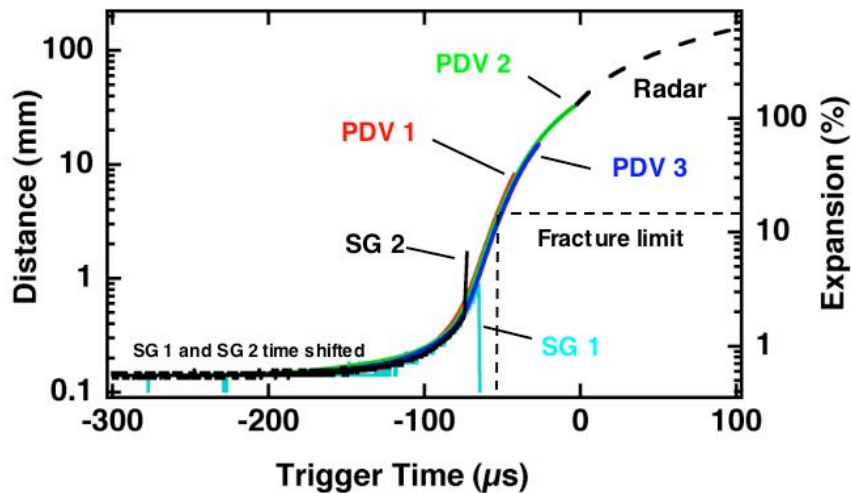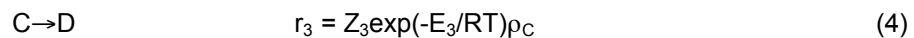

Figure 6 Tube wall motion measurements from strain gauges SG1, SG2, PDV, and radar for STEX test TE-047 with LX-10 confined in an AerMet 100 vessel

LX-10 model

ALE3D chemical, mechanical, and thermal models have been developed to model the cookoff of LX-10 in the STEX test (TE-047) described above. The decomposition of HMX in the LX-10 is modeled by four-step, five-species chemical kinetics based on the model reported by Tarver[10]. The first two steps are endothermic and the final two steps are exothermic.

$$A \rightarrow B \qquad\qquad r_1 = Z_1 \exp(-E_1/RT)\rho_A \tag{2}$$

$$B \rightarrow C \qquad\qquad r_2 = Z_2 \exp(-E_2/RT)\rho_B \tag{3}$$

$$C \rightarrow D \qquad\qquad r_3 = Z_3 \exp(-E_3/RT)\rho_C \tag{4}$$

$$D \rightarrow E \qquad\qquad r_4 = Z_4 \exp(-E_4/RT)\rho_D^2 \tag{5}$$

The decomposition of Viton A is represented by a single-step endothermic reaction.

$$A \rightarrow B \qquad\qquad r_5 = Z_5 \exp(-E_5/RT)\rho_A \qquad\qquad (6)$$

Here ρ_i is the mass concentration of a reactant i. The quantities r_j, Z_j, and E_j are the reaction rate, frequency factor and activation energy, respectively, for a reaction j. The components A and B are the solid species β- and δ-HMX, C is a solid intermediate, and D and E are intermediate and final gas products. The species A is solid Viton and B is the gaseous final product. The two reaction sequences are treated as non-interacting. The determination of the chemical kinetics parameters is described below.

After the Arrhenius reaction rates have increased to the point where changes are occurring on the time scale of sound propagation, a switch is made to a burn front model in which reactants are converted to products in a single reaction step. This switch in models is made for two reasons. The first is that the computational capabilities and methods are not yet available to resolve reaction zones which can be on the scale of nanometers. The second reason is that Arrhenius kinetics measured on the time scale of 1-10^4 s in the ODTX apparatus may not apply on shorter time scales. It is likely that deflagration rates measured in the strand burner described below provide a better measure of reaction behavior on short time scales. We assume that the burn front velocity, V, is a function of the pressure, p, at the front location, and use power-law expressions of the form to describe segments of the burn front curve:

$$V = V_0(p/p_0)^n \qquad\qquad (7)$$

Here the subscript 0 indicates a reference quantity. The selection of parameters for LX-10 is discussed below in the section on burn rates.

The mechanical behavior of the condensed HE constituents (HMX A, HMX B, HMX C) along with the Viton reactant (Viton A) is represented by Steinberg-Guinan mechanical models with a 7-term polynomial equation of state. The constant volume heat capacity does not vary with temperature in this EOS. Calculated melt and cold curves are used to account for the influence of compression on melting energy. A nonlinear regression[12] procedure was used to determine the coefficients that give an optimal representation of the measurements of the thermal expansion, compressibility, sound speed, and the unreacted shock Hugoniot.

The model gas constituents (HMX D, HMX E, Viton B) along with the air in the gap are treated as no-strength materials with gamma-law equations of state. This equation of state provides an approximate representation over much of the pressure range, except at the higher pressures of 10 kbar (1 GPa) where the model may be less accurate. The Γ-value for the HE gas species is set using a pressure of 1 kbar (100 MPa), a temperature of 2273°K, and the density and heat capacity from the thermo-chemical equilibrium computer code, CHEETAH 2.0[16] for the final product gases.

The time-dependent thermal transport model includes the effects of conduction, reaction, advection, and compression. The constant-volume heat capacity is constant for each reactant consistent with the Steinberg-Guinan model. The thermal conductivity for the condensed species A and B is taken to be constant, whereas the effects of temperature are included for the gaseous species. The heat capacity for the gases is assigned the same constant-volume value used in the gamma-law model. The temperature-dependent thermal conductivity is estimated at 1 kbar (100 MPa) using Bridgman's[17] equation for liquids in which the sound velocity is calculated using results from CHEETAH.

One-Dimensional-Time-to-Explosion (ODTX)

The materials parameters for the above models were assembled from measurements obtained for LX-10 samples investigated in earlier studies[18]. Two sets of ODTX measurements were made for LX-10 using the standard apparatus at LLNL (see Figure 7). In this system, the outer surface temperature of a 1.27 cm diameter sphere of HE is suddenly increased to a higher set-point temperature. The time to explosion is the time elapsed from the start of heating until confinement failure. The measurements of this study are plotted as a function of temperature in Figure 7.

Calculated explosion times for LX-10 are also shown in Figure 7 for a one-dimensional model involving transient heat conduction and the two chemical reaction sequences (Eqs. (2)-(5) for HMX and Eq. (6) for Viton). The two sets of experimental measurements are well represented by the ALE3D thermochemical model.

Burn rate measurements and model

The deflagration rate of LX-10 was measured with the LLNL High Pressure Strand Burner [19]. This system measures pressure during the burn and also the progress of the burn front with wires that melt as the flame advances. Cylindrical samples 6.4 mm diameter x 5.7 cm long are prepared by stacking nine pieces to form a burn tower. Temporal pressure data along with time of arrival data at each burn wire provide the information to calculate burn rate as a function of pressure.

The deflagration rate measurements are plotted versus pressure in Figure 8 for samples burned at room temperature. It is seen that the burn rates are high and have considerable scatter. Below approximately 100 MPa the measurements seem to follow a single curve, suggesting a smooth laminar burn. Also shown are measurements for LX-04 which follow the data for LX-10 very closely.   At higher pressures many of the LX-10 data points are larger by as much as three orders of magnitude than the values on the laminar burn curve for LX-04 (85% HMX, 15% Viton A). We believe that the samples of LX-10 are deconsolidating at the higher pressures which leads to increased surface area and a much higher effective burn rate. It seems that the increased binder in LX-04 is retarding the deconsolidation as the measurements follow single straight line. The LX-10 burn rate measurements are represented by one power-law burn rate model (see Eq. (7)) with n=1 in the laminar burn region below approximately 200 MPa. It is an open question as to how to represent the behavior of LX-10 in the deconsolidation region. We use a second power-law model with a steeper slope of n=6.4 which passes through the middle of the measurements in the deconsolidation region.
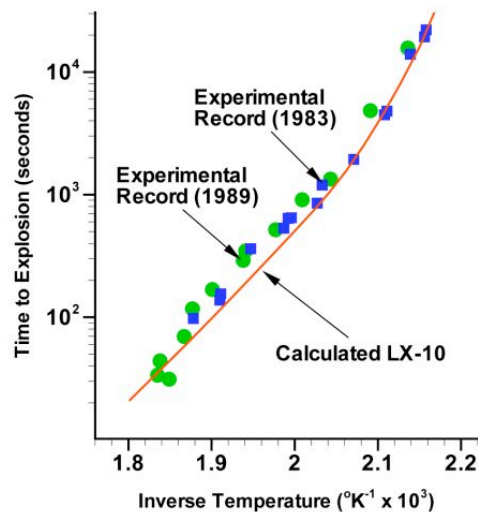

Figure 7. Comparison of model and measured ODTX explosion times as a function of temperature for LX-10.

An important remaining question concerns the effect of thermal damage. The burn rate measurements of Figure 8 were made for pristine samples at room temperature. The LX-10 sample for the above STEX experiment was heated slowly to ignition over approximately 3 days in the course of the test. This sample was certainly altered from its pristine condition. An investigation is in progress to determine the effects of this thermal damage on violence.

Boundary Conditions and Numerical Method

A two-dimensional, axisymmetric ALE3D model is used to simulate the cookoff of LX-10 in cookoff Test TE-047.   Boundary conditions for this model are shown schematically in Figure 1.   The two-dimensional model includes 8.66% ullage by volume on the HE side and no ullage on the end. In the experiment, the ullage was distributed over the sides and ends. In the simulation, the ullage is applied entirely to the sides to minimize the artificial pressurization resulting from numerical artifacts associated with the modeling of the gap. The gap is filled with air described by a gamma-law model in which the constant volume heat capacity is increased by a factor of 10 above its physical value to reduce spurious

temperature increases associated with rapid compression.   The HE and air do not slip at the wall, and all components of the vessel assembly are taken to be perfectly joined.
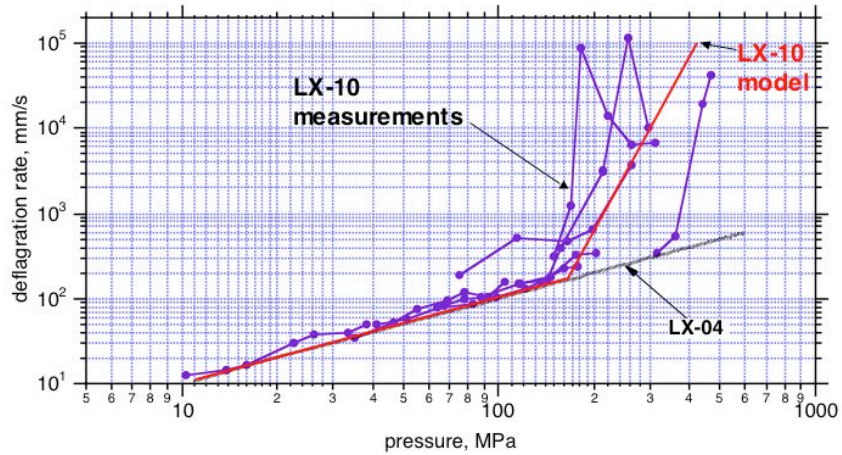

Figure 8. Comparison of model and measured burn rates as a function of pressure for LX-10 and LX-04.

The top, bottom, and side heaters are applied as uniform heat flux conditions on the top, bottom, and side surfaces. Included among the side heater surfaces are the sides of the tube and flanges along with the inward facing surfaces of the flanges (see Figure 1). The heat fluxes for these three heaters are adjusted using three independent PI controllers to maintain the temperatures TC1, TC2, and TC3 at their set-point values. Thermal convection is applied to all outward facing surfaces using heat transfer coefficients for laminar flow of air past appropriate model surfaces such as vertical and horizontal plates[20]. Standard expressions for hemispherical radiation are used on these same surfaces.   A boundary layer expression for heat transfer resulting from the flow of air past a vertical plate is used on the tube surface. This expression has a dependence on the vertical coordinate, and is used to compensate for preferential cooling observed on the lower portion of the tube. During the final ramp of 1° C/h, the upper and lower control temperatures TC2 and TC3 are kept 9 and 4 °C cooler than the side control temperature in an attempt to keep the ignition point near the axial midplane (see Figure 1).

The ALE3D computer code requires 3D meshes, and a wedge-shaped mesh is employed for the 2D model of this study. A small hole is present near the symmetry axis to allow the use of hexahedral elements at all locations. In the base case, the tube cavity has 12 elements in the radial direction which is increased by a factor of 2 in mesh refinement studies. Some of the elements have both HE and air, and standard mixing rules are employed to calculate the energy, heat capacity, thermal conductivity, shear modulus, and equation of state[21]. The mesh is smoothed using a combination of Lagrange and Eulerian algorithms. Nodes initially on the interface between the cavity and the steel remain on these boundaries while nodes interior to the cavity are advected through the flowing HE and air.

A fully implicit method is used for the integration of the thermal transport equations during the thermal ramp and much of the subsequent ignition process. After the time step has decreased to within a factor of 10 of the value given by the Courant condition, a switch is made from implicit to explicit integration of the thermal transport equation.   During the thermal ramp and subsequent ignition process, the hydrodynamic equations are integrated using an explicit method with the material densities increased by a large factor to make the calculations computationally feasible. An algorithm is used to select the scale factor. During thermal runaway, the time step is decreased by approximately 14 orders of magnitude to resolve behavior on the dramatically shrinking time scale.

After a temperature reaches a user-specified threshold value, the multi-step kinetics model is replaced by the burn front expression (7). The burn front is propagated through the HE with the assumption that reactants are converted completely to products in a single step. This burn front is tracked using a level set method that conserves mass, momentum, and energy across the front.   Since the mesh is not moved to explicitly track the front, the resolution of the burn front is on the scale of the mesh element size. The effects of mesh size are an important consideration under current investigation.

-9-

COMPARISON OF MODEL AND MEASURED COOKOFF RESULTS

In cookoff Test TE-047 for LX-10, the set-point temperature for TC1 was increased from room temperature to 130°C, held for 5.0 h, and then increased at 1°C/h until cookoff (see Figures 1 and 2). The measured center internal temperature TC6 shows a dip around 155 °C which is associated with the β to δ phase transition for HMX. After the hold at 130°C, the top and bottom set-point temperatures TC2 and TC3 are kept 9 °C and 4 °C cooler than TC1, respectively. The cookoff temperature, taken to be the set-point temperature at the end of runaway, is 182 °C for both the simulation and experiment, indicating that the model provides an excellent prediction (see Figure 2). Both the measured and model internal temperatures begin to increase 2 h before ignition.

Initial experimental and model hoop strain results for SG1 are shown for the duration of the test in Figure 9. The location for the measurement is the side of the vessel at the axial midplane (see Figure 1). On the 70 h time scale of the test, the strain measured on long times shows linear increases that follow the changes in temperature. This suggests that the increases in measured strain follow the thermal expansion of the tube. At ignition, there is a rapid increase in strain to 3.4% based on the measurements at a high sampling rate (see Figure 6). The simulated strains for the 1X and 2X meshes, approximately track the measured values until t=40 h at which time there is a more rapid increase in the model curves. The model results are approaching the measured results as the mesh is refined. The discrepancies observed are likely the result of mass scaling, the model representation of the gap using mixed materials, and possibly flaws in the chemical kinetics models as has been noted in earlier studies[3, 22]. In the future, more detailed comparisons will be made between model calculations and the measured strains, the PDV curves, and radar measurements described above.
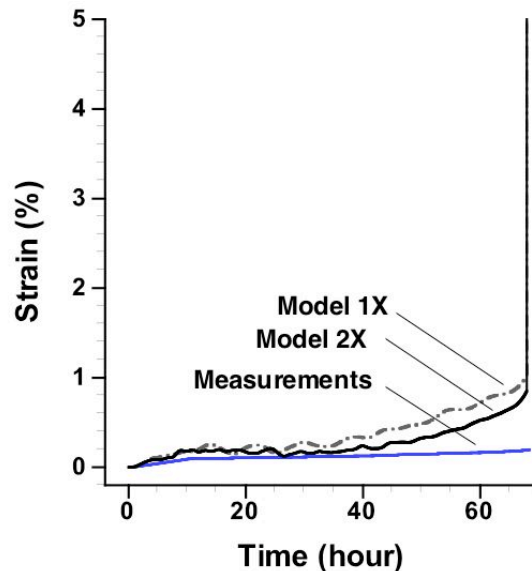

Figure 9. Comparison of model and measured strain rates for STEX test TE-047 with LX-10 confined in an AerMet 100 vessel

FRAGMENTATION OF AERMET 100 TUBES FROM DEFLAGRATION OF LX-10

Detailed ALE3D fragmentation models are being developed to allow violence to be predicted during later stages of thermal explosions. Since the wall velocity and position curves of Figures 5 and 6 show considerable acceleration of the fragments after fracture, a detailed model of fracture and fragmentation may be needed for the prediction of violence.

The fracture of AerMet 100 tubes is investigated in two model problems involving the deflagration of LX-10. In the first problem, the LX-10 is confined in an AerMet 100 tube (10.16 cm L x 5.08 cm OD) with a 3 mm wall thickness. This tube is selected to be half the length of the tube employed in the STEX test in order to reduce computation time. The mesh has 1/4 symmetry with 1 million zones approximately

250 μm in dimension. In order to conserve computation time and focus on the fracture behavior resulting from deflagration, the problem is artificially initiated by starting the deflagration at the center of the system. The deflagration front propagates outward, pressurizing and then fracturing the vessel as shown in Figure 10. Zones near the axial midplane fail first, and the resulting cracks propagate towards the ends of the tubes. The calculation fails when gases flowing into the cracks cause excessive deformation in the failure zones. It is seen that the fragments range from a few millimeters to approximately a centimeter in size.   A baseline set of parameters is being used for the Johnson-Cook model. These parameters may need to be modified to provide a good description of the measured fragment size distribution for the LX-10 STEX test.

A second test problem was used to examine the effects of varying the Gaussian failure strain distribution in the Johnson-Cook model. This distribution for the parameter D_1 in Equation (1) is varied from ±10% to ±30%. The LX-10 is confined in a short AerMet 100 tube section (2.54 cm L x 5.08 cm OD) with a 3 mm wall thickness. This geometry is selected to minimize the computation time, but leave a large enough domain to provide a statistically significant fragment size distribution.   Zone sizes are similar to the 250 μm size of the first test problem for fragmentation. The simulation begins with a deflagration of the LX-10 at the midplane on the axis of symmetry as described above. As the variation in D_1 is increased, the fragment sizes increase from nominally 2-3 mm to approximately 7-8 mm in size. In future work, fragment sizes for complete cookoff calculations will be compared in detail with measured distributions. The fragment sizes at the high end of the range are of the same scale as the measured 1-2 cm fragment size.
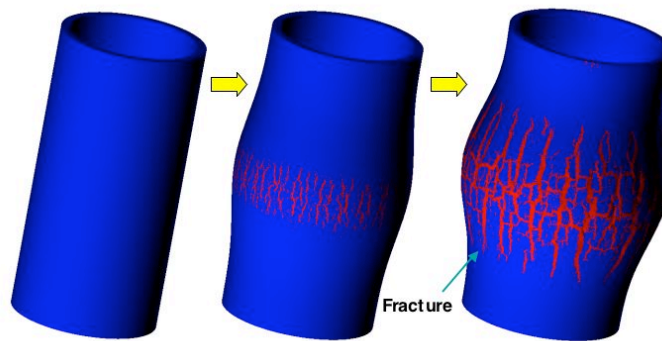

Figure 10. Deflagration-driven fracture of AerMet 100 tube. The deflagration starts at the center of the LX-10 cylinder (not shown) and propagates towards the tube wall. The failure zones (cracks) are in red and the metal is blue.
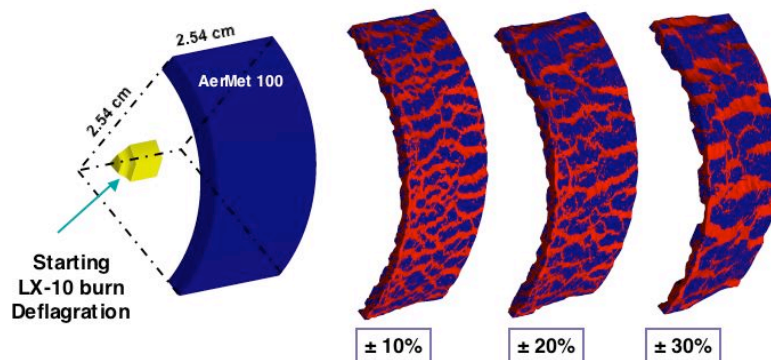

Figure 11. Deflagration-driven fracture of AerMet 100 tubes. The deflagration starts at the center of the LX-10 cylinder (not shown) and propagates towards the tube wall. The indicated variations are for a Gaussian distribution of failure strains. The failure zones (cracks) are in red and the metal is blue.

CONCLUSIONS

An experimental and numerical investigation was performed to characterize violence for the slow cookoff of LX-10 confined in a 5.08 cm diameter AerMet 100 vessel. This benchmark STEX experiment included several diagnostic systems to measure violence at various stages of the thermal explosion. Measurements from strain gauges, three PDV probes, and micropower radar units were combined to construct a single plot of wall position versus time for 15 cm of motion. Approximately 78% of the AerMet 100 tube was recovered as loose fragments and fragments imbedded in Lexan panels. A fragment size distribution was constructed for the 106 fragments. The median fragment mass was 2.2 g, and fragments were of the scale 2 cm in size. Based on measurements of fragment thickness, the real strain at failure was approximately 15%. The explosion was a violent deflagration based on the average radar velocity of 1200 m/s, the 200 μs time scale of the explosion, and the measured fragment sizes.

We performed ALE3D simulations for this cookoff test. The mechanical behavior of the AerMet 100 was represented by Steinberg-Guinan models with a Gruneisen EOS. A Steinberg-Guinan mechanical model with polynomial EOS was used for the HMX and Viton solid species while Gamma-Law models were selected for the gases. A four-step Tarver-McGuire model was used to represent the chemical kinetics behavior at long times based on ODTX measurements. The power-law burn model was employed for the microsecond time scale to represent measurements made with the high-pressure-strand burner. The prediction for the STEX explosion temperature was in excellent agreement with the measured value. However, the predicted strains were significantly larger than the measured values. Possible contributing factors include the numerical errors associated with mass scaling, the representation of the gap, and errors in the decomposition model. The numerical errors are expected to be reduced with the completion of an implicit integration algorithm for the momentum equation.

ALE3D models were applied to test problems for the fragmentation of AerMet 100 tubes driven by the deflagration of confined LX-10. The fragmentation was described by a Johnson-Cook model with a distribution for failure strains. The results show the generation of cracks and fragments at conditions similar to those in the completed STEX test. In addition, parameters in the failure strain distribution were varied to determine the effect on fragment size.

ACKNOWLEDGMENTS

REFERENCES

1. Nichols, A. L., A. Anderson, R. Neely and B. Wallin, "A Model for High Explosive Cookoff," Proceedings of 12th International Detonation Symposium, San Diego, CA, 2002.

2. Maienschein, J. L. and J. F. Wardell, "The Scaled Thermal Explosion Experiment," Proceedings of 12th International Detonation Symposium, San Diego, CA, 2002.

3. Yoh, J. J., M. A. McClelland, J. L. Maienschein, J. F. Wardell and C. M. Tarver, "Simulating thermal explosion of cyclotrimethylenetrinitramine-based explosive: Model comparison with experiment," *J. Appl. Phys.*, vol. 97, pp. 083504-1-11, 2005.

4. Erikson, W. W. and R. G. Schmitt, "Modeling Thermal Decomposition and Deflagration in Small and Munition-Scale Navy Cookoff Experiments," Proceedings of JANNAF 39th Combustion and 21st Propulsion Systems Hazards Subcommittee Meetings, Colorado Springs, CO, 2003.

5. Atwood, A. I., P. O. Curran, M. W. Decker and T. L. Boggs, "Experiments for Cookoff Model Validation," Proceedings of JANNAF 37th Combustion and 19th Propulsion Systems Hazards Subcommittee Meetings, Monterey, CA, CPIA, 2000.

6. Atwood, A. I., P. O. Curran, R. Heindahl, W. W. Erikson and M. J. Kaneshige, "Full Scale Model Validation Experiments," Proceedings of JANNAF 39th Combustion and 21st Propulsion Systems Hazards Subcommittee Meetings, Colorado Springs, CO, 2003.

7. Sandusky, H. W., "Follow-on to NSWC Cookoff Validation Experiments," Proceedings of JANNAF 39th Combustion and 21st Propulsion Systems Hazards Subcommittee Meetings, Colorado Springs, CO, 2003.

8. McClelland, M. A., T. D. Tran, B. J. Cunningham, R. K. Weese and J. L. Maienschein, "Cookoff Response of PBXN-109: Material Characterization and ALE3D Thermal Predictions," Proceedings of 50th JANNAF Propulsion Meeting, Salt Lake City, UT, CPIA, 2001.

9. McClelland, M. A., J. L. Maienschein, J. E. Reaugh, T. D. Tran, A. L. Nichols and J. F. Wardell, "ALE3D Model Predictions and Experimental Analysis of the Cookoff Response of Comp B," Proceedings of JANNAF 39th Combustion and 21st Propulsion Systems Hazards Subcommittee Meetings, Colorado Springs, CO, 2003.

10. Tarver, C. M. and T. D. Tran, " Thermal decomposition models for HMX-based plastic bonded explosives " *Combustion and Flame*, vol. 137, pp. 50-62, 2004.

11. Orzechowski, T. J., M. B. Aufderheide, R. C. Becker, P. J. Bedrossian, D. M. Goto, H. K. Springer, A. J. Sunwoo and C. K. Syn, "Joint DoD/DOE Munitions Technology Development Program FY-02 Progress Report, Dynamic Fracture and Fragmentation of Metals," UCRL-ID-103482-02, 2003.

12. McClelland, M. A., J. L. Maienschein and A. L. Nichols, "Joint DoD/DOE Munitions Technology Development Program FY-01 Progress Report, Ignition and Initiation Phenomena: Cookoff Violence Prediction," Lawrence Livermore National Laboratory, 2002.

13. Couch, R., D. Nikkel, R. C. Becker, T. Dunn, D. M. Goto, H. K. Springer, D. Lassila and K. Whittaker, "Joint DoD/DOE Munitions Technology Development Program FY-02 Progress Report, 3D Computations and Experiments," UCRL-ID-103482-02, 2003.

14. Johnson, G. R. and W. H. Cook, "Fracture characteristics of three metals subjected to various strains, strain rates, temperatures, and pressures," *Engineering Fracture Mechanics*, vol. 21, pp. 38-41, 1985.

15. Hancock, J. W. and A. C. McKenzie, "On the mechanism of ductile failure in high strength-steels subjected to multi-axial stress states," *J. Mech. Phys. Solids*, vol. pp. 147-169, 1976.

16. Fried, L. E., W. M. Howard and P. C. Souers, "Cheetah 2.0 User's Manual," Lawrence Livermore National Laboratories, UCRL-MA-117541 Rev. 5, 1998.

17. Bird, R. B., W. E. Stewart and E. N. Lightfoot, *Transport Phenomena,* Wiley, pp. 260-261, 1960.

18. Tran, T. D., "A Complilation of One-Dimensional, Time-to-Explosion (ODTX) Data for High Explosives and Propellants," Lawrence Livermore National Laboratory, UCRL-ID-151449, 2003.

19. Maienschein, J. L. and J. B. Chandler, "Burn Rates of Pristine and Degraded Explosives at Elevated Pressures and Temperatures," Proceedings of 11th International Detonation Symposium, Snowmass, CO, Office of Naval Research, 1998.

20. Holman, J. P., *Heat Transfer,* McGraw-Hill, pp. 253-254, 1976.

21. Sharp, R., "Users Manual for ALE3D An Arbritrary Lagrange/Eulerian 3D Code System," Lawrence Livermore National Laboratory, 2003.

22. Yoh, J. J., M. A. McClelland, J. L. Maienschein and J. F. Wardell, "Towards a predictive thermal explosion model for energetic materials," *J. Comp.-Aided Matls. Design*, vol. 10, pp. 175-179, 2005.